Virtual and Solution Conformations of Oligosaccharides†

Dale A. Cumming and Jeremy P. Carver*
Departments of Medical Genetics and Medical Biophysics, University of Toronto, Toronto, Ontario, Canada M5S 1A8
Received May 28, 1986; Revised Manuscript Received April 3, 1987

ABSTRACT: The possibility that observed nuclear Overhauser enhancements and bulk longitudinal relaxation times, parameters measured by ^{1}H NMR and often employed in determining the preferred solution conformation of biologically important molecules, are the result of averaging over many conformational states is quantitatively evaluated. Of particular interest was to ascertain whether certain ^{1}H NMR determined conformations are "virtual" in nature; i.e., the fraction of the population of molecules actually found at any time within the subset of conformational space defined as the "solution conformation" is vanishingly small. A statistical mechanics approach was utilized to calculate an ensemble average relaxation matrix from which $\langle$NOE$\rangle$'s and $\langle T_1\rangle$'s are calculated. Model glycosidic linkages in four oligosaccharides were studied. The solution conformation at any glycosidic linkage is properly represented by a normalized, Boltzmann distribution of conformers generated from an appropriate potential energy surface. The nature of the resultant population distributions is such that 50% of the molecular population is found within 1% of available microstates, while 99% of the molecular population occupies about 10% of the ensemble microstates, a number roughly equal to that sterically allowed. From this analysis we conclude that in many cases quantitative interpretation of NMR relaxation data, which attempts to define a single set of allowable torsion angle values consistent with the observed data, will lead to solution conformations that are either virtual or reflect torsion angle values possessed by a minority of the molecular population. On the other hand, calculation of ensemble average NMR relaxation data yields values in agreement with experimental results. Observed values of NMR relaxation data are the result of the complex interdependence of the population distribution and NOE (or T_1) surfaces in conformational space. In conformational analyses, NMR data can therefore be used to test different population distributions calculated from empirical potential energy functions.

The utility of nuclear magnetic resonance spectroscopy (NMR)[1] in determining interatomic distances resides in the fact that various spectral attributes (e.g., coupling constants and relaxation parameters) are dependent upon the geometry of the spin system under study. In particular, the dominance of dipole–dipole (DD) relaxation in solution ^{1}H NMR studies, when coupled with the r^{-6} dependence of this relaxation process (Bloembergen, 1971), provides an indispensible tool for probing molecular geometries. Nuclear Overhauser enhancements (NOE's) are an elegant and sensitive method for the assessment of DD relaxation processes, thus explaining their widespread use in conformational analyses. Strictly speaking, however, the formulation of NOE theory most widely used is applicable only to molecules considered to be rigid in solution (Noggle & Schirmer, 1971).

The problem of internal motions (motions in a molecule that do not involve the breaking of covalent bonds) presents serious difficulties in the interpretation of NMR relaxation data. The basic problem lies in the fact that nuclear magnetic relaxation is dependent upon molecular motions, yet the nature of these motions cannot be derived directly from NMR data. Instead, one is restricted to postulating motional models that are considered acceptable as long as "correct" predictions of relaxation data are made. A number of attempts have been made to explicitly include the effects of internal motion, in calculating not only NOE's (Noggle & Schirmer, 1971; Gueron et al., 1973; Keepers & James, 1982) but also nuclear magnetic relaxation in general [for a comprehensive discussion, see Jardetzky and Roberts (1981)]. In the absence of appropriate consideration of internal motion, an "average" conformer is derived from NMR data due to contributions from n number of individual conformers. Since the population of molecules is distributed among at least n individual conformational states, few, if any, molecules possess the "average" conformation; these NMR-derived results are, therefore, termed "virtual" conformations (Jardetzky, 1980).

Fortunately, there are situations where it is possible to deal with the problem of internal motions without substantially altering the basic formulation of DD relaxation. In one such case, internal motions do not affect internuclear distances (e.g., motion of a methyl group), and a general formulation explicitly incorporating these motions into the effective tumbling time of the molecule has been put forward (Woessner et al., 1969). Further, Noggle and Schirmer (1971) have considered two cases where the rate of internal motion (k, which we will characterize as the inverse of the correlation time of internal motion, τ_i) is slow relative to the molecular tumbling time. In their first case, internal motion is very slow ($\tau_c < T_1 \ll \tau_i$) compared to the rate of NOE buildup (on the order of T_1) such that during steady-state experiments (such as NOE experiments) a fraction of the molecules in each conformation is "frozen" long enough to independently come to the steady-state condition. When NOE experiments are performed under these conditions, the observed enhancement on any spin d upon

† This research was supported by Grants MT-3722 and MA-6499 from the Medical Research Council of Canada.
* Address correspondence to this author.

[1] Abbreviations: NMR, nuclear magnetic resonance spectroscopy; NOE, nuclear Overhauser enhancement; DD, dipole–dipole; r, internuclear distance; Man, D-mannopyranose; GlcNAc, 2-acetamido-2-deoxy-D-glucopyranose; Q, partition function; F, minimum fraction of ensemble microstates defining a specified probability; $\langle X\rangle$, ensemble averaged observable; Y{X}, NOE observed on nucleus Y upon irradiation of nucleus X; T_1, bulk longitudinal relaxation time; MPL, maximum (normalized) probability for any microstate in an ensemble.

0006-2960/87/0426-6664$01.50/0

saturations of spin s is then the ensemble average of steady-state NOE's. In their second example, the rate of internal motion is "moderate" ($\tau_c < \tau_i < T_1$): the residence time in any conformation is short compared to the time required for the equilibrium NOE to be established such that all conformations are sampled by all molecules, and thus, they all approach the same steady state. Unlike the first case, the steady-state NOE will depend on the ensemble average value of r^{-6}. It is this latter case that is applicable to the motions studied in this paper.

During recent studies on the solution conformation of N-linked glycans, we have noted a number of cases where the NMR-defined solution conformation did not correspond to any (or only one of several) potential energy minima. Two possibilities could account for this observation. Either the molecules in solution were undergoing some form of internal motion and the experimentally observed NOE's and T_1's were the result of averaging over multiple conformational states during the time course of the NMR experiment, or important interaction terms were not being considered during potential energy calculations. The former possibility is the focus of this paper while the latter possibility is dealt with in the following paper (Cumming & Carver, 1987).

Experimental Procedures

A Statistical Mechanics Formulation. For the *j*th glycosidic linkage in a glycan (containing *n* glycosidic linkages: 1, 2, *j*, ..., *n*), we define an ensemble of conformational microstates, Ω_j, whose coordinate axes are defined by the "appropriate" glycosidic torsional angles, those which affect the value of the potential energy upon rotation for the *j*th linkage. In disaccharides, appropriate torsion angles are usually ϕ and ψ (and ω if the linkage is 1,6), while in larger glycans it is desirable to identify any additional appropriate torsion angles. For the remainder of this formulation, it will be assumed that the appropriate torsion angles are only those of the *j*th linkage, although inclusion of additional angles is straightforward, and hence, we drop the subscript *j* for simplicity. Since a continuum of values for ϕ, ψ, and ω represents all possible conformational states of a linkage, Ω is a subset of the *n*-dimensional conformational surface where discrete values for the torsional angles serve to approximate the overall surface. The energy of the *i*th conformational microstate of Ω, $E_i(\phi,\psi,\omega)$, is calculated by potential energy algorithms. The relative population (probability) of the *i*th conformational microstate P_i is governed by the Boltzmann distribution such that

$$P_i = \exp[-(E_i(\phi,\psi,\omega)/kT)]/Q$$

where Q, the "classical" partition function, is given by

$$Q = \sum_i \exp[-(E_i(\phi,\psi,\omega)/kT)]$$

and thus

$$\sum_i P_i = 1$$

Moreover, a cross-relaxation matrix, S_i, can be calculated for each microstate. As defined previously [e.g., Carver et al. (1987)], the cross-relaxation matrix is a subset of the total nuclear magnetic relaxation matrix from which the row corresponding to the saturated hydrogen in an NOE experiment has been deleted. The elements of S_i, $\sigma_i kl$, are dependent only upon the intrinsic spin geometry (in terms of interatomic distances) and the spectral density function for specified values of ϕ, ψ, and ω and are calculated as before (Brisson & Carver, 1982a). An ensemble average cross-relaxation matrix is then defined as

$$\langle S \rangle = \sum_i P_i S_i$$

$\langle S \rangle$ is then utilized to solve the series of simultaneous equations defined by Noggle and Schirmer (1971) to calculate NOE's:

$$\langle R_d \rangle \langle f(d,s) \rangle + \sum_{k \neq d} \langle \sigma_{dk} \rangle \langle f(k,s) \rangle = \langle \sigma_{ds} \rangle$$

where R_d is the DD relaxation rate for the "detected" spin in the absence of cross-relaxation and $f(d,s)$ and $f(k,s)$ are the enhancements for the d and k spins on saturation of spin s. Similarly, $\langle S \rangle$ is utilized to calculate bulk T_1's (Dais et al., 1984), where

$$1/\langle T_1 \rangle = \langle R_k \rangle + \sum_{k \neq 1} \langle \sigma_{kl} \rangle$$

NOE's and T_1's calculated from $\langle S \rangle$ are ensemble averages and are denoted $\langle$NOE$\rangle$ and $\langle T_1 \rangle$. The isotropic rotational correlation time is assumed to be identical for all conformational microstates. Since the rate of internal motion is slow compared to the overall molecular correlation time, this seems to be a reasonable assumption for these small molecules. To represent the ϕ, ψ, ω surface as an ensemble of discreet microstates and to make calculations computationally reasonable, a 60 × 60 × 60 array of ϕ, ψ, and ω values, incremented 5° per element, was constructed yielding a total of 2.16 × 10^5 microstates per 1,6 linkage. The 60° range along each angular dimension excluded from these calculations was selected from a region of highly unfavorable steric interactions such that the effect on ensemble properties was negligible. For 1,2, 1,3, or 1,4 linkages, two-dimensional ensembles were generated over 360° in each dimension, either at 3° (120 × 120) or 6° (60 × 60) resolution. All calculations reported in this paper involved variations of a single set of linkage angles. Clearly, extensions to larger ensembles would be more appropriate but rapidly become too demanding computationally.

^1H NMR Spectroscopy. Details for the preparation of samples and acquisition of T_1 and NOE data are identical with those given in the first paper in this series (Cumming et al., 1987).

Other Computational Procedures. The four potential energy algorithms employed in this study are simple derivatives of the program HSEA (Lemieux et al., 1980; Thorgersen et al., 1982). The HSEA program, our first algorithm, calculates the contributions to the potential energy from two components: nonbonded interactions (hard sphere, HS) calculated with the Kitaigorodsky expression (Kitaigorodsky, 1978, 1961) using the parameterization of Venkatachalam and Ramachandran (1967) and contributions from the exo-anomeric effect (EA) calculated with a three-term decomposed Fourier expansion modeling the differences between ab initio calculations and nonbonded interactions in the torsion potentials of dimethoxymethane (Thorgersen et al., 1982). Our second algorithm HEAH is the HSEA program described above plus the hydrogen-bonding potential of Serge Perez (Mackie et al., 1986). This algorithm calculates hydrogen-bonding energies (in kcal/mol) according to the empirical expression

$$E_{hb} = 33.14(R - 2.55)(R - 3.05)$$

where R is the internuclear distance between heteroatoms separated by distances between 2.55 and 3.05 Å. As coded in our algorithm, only contributions between appropriate pairs of heteroatoms are allowed. Our third algorithm HSEL utilizes the algorithm for nonbonded interactions described above plus contributions from electrostatic effects calculated as the sum of pairwise Coulombic interactions between partially charged atoms. Values for the fractional charges on

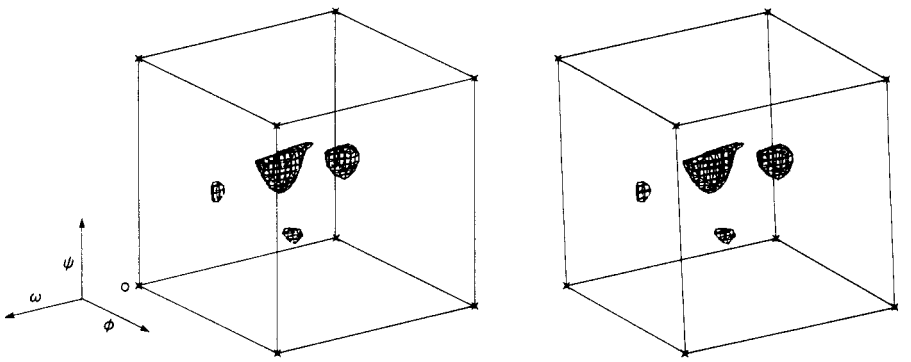

FIGURE 1: Three-dimensional contour surfaces representing the 50% population level in calculated ensembles for Man(α1,6)Man(β)OMe. Potential energy values for each microstate in three-dimensional conformational space, for rotation about the α1,6 linkage, were calculated with the noted algorithm as described under Experimental Procedures. Contour surfaces were constructed by plotting the potential energy value equal to a given threshold value. This threshold value for each diagram was calculated, as described in the text, such that generated volumes are inclusive of 50% of the population of disaccharide molecules. The relative origin of the plot is located at the lower rear left section of the diagram (marked o) and represents the point ϕ, ψ, ω = −150°, 10°, 90°. Each axis extends 300° in each dimension with a positive direction noted by the axes. In the remainder of the legend, MPL denotes the maximum (normalized) probability for any microstate in the ensemble. The figure represents the results calculated with the HSEA potential energy algorithm: global minimum, −2.2 kcal/mol; MPL, 0.140%; threshold energy level, −0.8 kcal/mol. For the other three calculated ensembles (not shown) the following results were obtained: (HEAH) global minimum, −2.9 kcal/mol; MPL, 0.382%; threshold energy level, −0.8 kcal/mol; (HSEL) global minimum, −5.3 kcal/mol; MPL, 0.083%; threshold energy level, −4.0 kcal/mol; (HSEH) global minimum, −6.6 kcal/mol; MPL, 0.660%; threshold energy level, −4.0 kcal/mol.

atoms were taken from the data of Potenzone and Hopfinger (1975). The fourth algorithm HSEH is the HSEL algorithm with hydrogen-bond interactions included as described above. Electrostatic and exo-anomeric contributions were never evaluated in the same algorithm since the exo-anomeric effect is electrostatic in origin; hydrogen-bonding and electrostatic contributions were calculated together since our algorithms do not explicitly reorient hydroxyls and the resulting overlap is negligible. Stereo three-dimensional contour surfaces were generated with a FORTRAN routine made available by Dr. Karl Hardman (Naval Research Laboratory, Washington, DC) and subsequently adapted for this data by James Rini and Thomas Lew in this laboratory. Computer programs to calculate ensemble average NOE's and T_1's were written in DCL (DEC Command Language, Digital Electronics Corp.) and executed, as were all other programs, on a VAX 11/780 located at the Ontario Cancer Institute. VAX/VMS source code listings for programs calculating ensemble-averaged NMR relaxation data are available from the authors upon request.

Sample Sources. All model compounds utilized in this paper were synthesized as described elsewhere (Shah et al., 1986; Shah et al., unpublished results).

Results

Evaluation of Ensemble Average NOE and T_1 Values. The lack of agreement between experimentally determined conformations and potential energy calculations for linkage conformations in a number of oligosaccharides suggested to us that extensive averaging among the conformations specified by potential energy minima might be occurring. To test this possibility, we have used a statistical mechanics formulation (outlined under Experimental Procedures) to calculate $\langle$NOE$\rangle$ and $\langle T_1 \rangle$ values for comparison with experimental values. Since the probability distribution among microstates will be dependent upon the nature of the potential energy surface, we can evaluate different potential energy algorithms for their ability to predict observed NMR data. For this purpose, we have used four potential energy functions which utilize different combinations of interaction terms: HSEL, HSEH, HSEA, and HEAH (see Experimental Procedures).

The Man(α1,6) Linkage. A three-dimensional potential energy array was calculated for the model compound Man(α1,6)Man(β)OMe (compound I), as a function of the three glycosidic torsion angles necessary to specify the 1,6 linkage conformation, with the four potential energy algorithms described under Experimental Procedures. For each algorithm, the resulting array defines an ensemble of microstates, Ω, in three-dimensional conformational space (a geometric space whose coordinate axes are defined by the three glycosidic torsion angles describing this linkage). Each Ω is therefore a static subset of n-dimensional conformational space, where n represents the total number of translational and rotational degrees of freedom. The corresponding Boltzmann population distribution among ensemble microstates can be calculated as described under Experimental Procedures. From the normalized population distribution it is possible to obtain the minimum energy configuration of microstates, which specifies a given fraction of the population (or probability) and the "threshhold" potential energy, which, if the fractional population of all microstates i (with E_i less than or equal to this threshold value) are summed, yields the specified fractional population. Figures 1 and 2 show the three-dimensional potential energy surfaces obtained by contouring a single energy value, the threshhold energy levels designating the 50 and 95% population levels, respectively, for the calculated ensembles. Therefore, the region enclosed by these "nets" describes the subset of conformational space within which 50 or 95% of the molecular population is found.

In Figure 1, the 50% threshhold potential energy value is drawn for the ensemble calculated with the HSEA algorithm, Ω[HSEA]. The bounded regions of Ω shown illustrate the general features of potential energy surfaces for 1,6 linkages described previously (Tvaroska et al., 1978). Possible values for ϕ are limited to a narrow region centered near ϕ = −50°. Along the ω axis, three subpopulations can be seen corresponding to the three possible staggered rotamers (ω = +60°, −60°, and 180°). For some values of ω, two subpopulations are notable along the ψ axis resulting from local distributions about minima at ψ = 95° and 200°. Essentially the same profile was obtained for Ω[HEAH]. Compared to Figure 1, the inclusion of a hydrogen-bond interaction term has the effect of generating a new global potential energy minimum (near ϕ, ψ, ω = −50°, 220°, 180°) but yields only minor effects on the overall appearance of the contour surface, as well as the population distribution in conformational space.

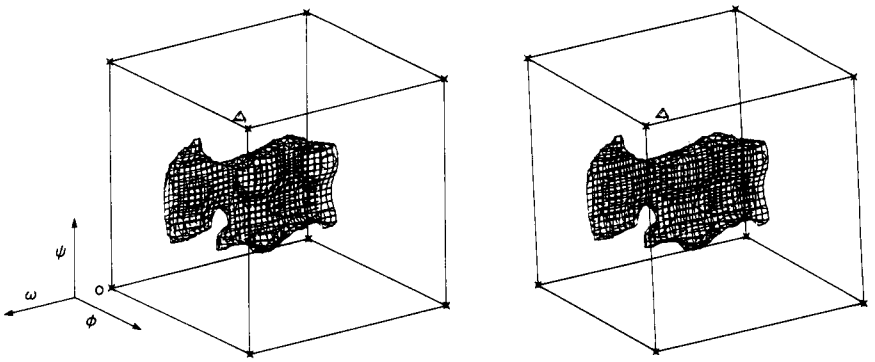

FIGURE 2: Three-dimensional contour surfaces representing the 95% population level in calculated ensembles for Man(α1,6)Man(β)OMe. Potential energy values were generated with the HSEA potential; essentially identical results were obtained with the other three algorithms. Details for the calculation of this stereo contour surface plot are identical with those given in the legend to Figure 1 except that the threshold energy level (+0.5 kcal/mol) was altered to yield a volume inclusive of 95% of the population.

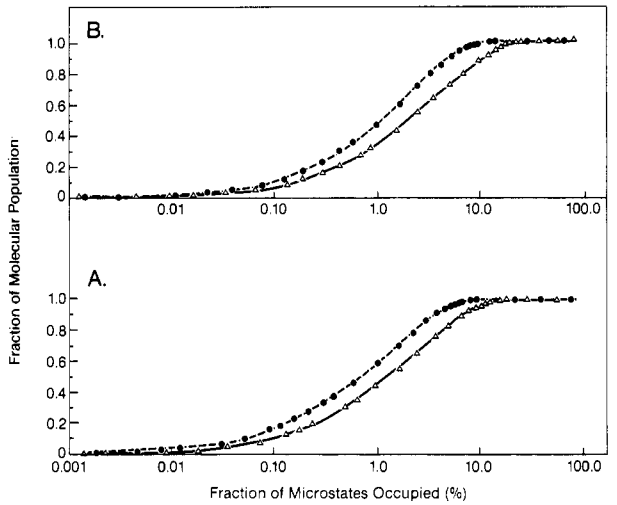

FIGURE 3: Population distribution among conformational microstates for two 1,6 linkages. Plots show the minimum fraction of the total number of ensemble lattice points (2.16×10^5) (considering lattice points in descending order of probability) necessary to account for a specified fraction of the population of disaccharide molecules. Alternatively, the x axis can be thought of as representing the minimum fraction of ensemble lattice points necessary to find a given molecule with the specified probability. (A) Man(α1,6)Man(β)OMe: (●) HSEA potential energy algorithm; (△) HSEL potential energy algorithm. (B) GlcNAc(β1,6)Man(α)OMe: (●) HSEA potential energy algorithm; (△) HSEL potential energy algorithm. For both disaccharides, inclusion of hydrogen-bonding interactions yielded only small changes in each curve (see Table I for further details).

Table I: Summary of Fitted Parameters a and b for Population Distributions Calculated from Various Potential Energy Algorithms[a,b]

sample	algorithm	a	b
Man(α1,6)Man(β)OMe (complete)	HSEL	0.97	0.93
	HSEH	0.88	0.67
	HSEA	0.57	0.93
	HEAH	0.53	0.79
Man(α1,6)Man(β)OMe (truncated)	HSEL	1.21	0.93
	HSEH	0.91	0.69
	HSEA	0.62	0.94
	HEAH	0.63	0.78
GlcNAc(β1,6)Man(α)OMe (complete)	HSEL	1.60	0.90
	HSEH	0.74	0.67
	HSEA	0.95	0.91
	HEAH	0.58	0.65
GlcNAc(β1,6)Man(α)OMe (truncated)	HSEL	1.88	0.96
	HSEH	0.86	0.70
	HSEA	0.97	0.95
	HEAH	0.69	0.68
GlcNAc(β1,2)Man(α)OMe	HSEL	0.88	1.02
	HSEH	0.82	1.05
	HSEA	0.63	1.44
	HEAH	0.17	1.11

[a] The parameters a and b are those defined in the equation $Y = 1/[1 + (a/X^b)]$, where Y is the fraction of the molecular population and X is the fraction of ensemble microstates occupied. a approximates the minimum fraction of microstates necessary to specify 50% of the molecular population and has been multiplied by 100 for expression as a fractional percentage in the table. [b] Correlation coefficient for the logistic fit.

Surprisingly, the bounded subset of Ω[HSEL] at the 50% probability level is also very similar to that shown in Figure 1; compared to the ensembles generated with the HSEA and HEAH algorithms, Ω[HSEL] possesses a global minimum 3 kcal/mol lower. Inclusion of a hydrogen-bond interaction term in calculating Ω[HSEH] also yields a similar pattern; however, in this case the global minimum is 4 kcal/mol lower than that in Ω[HEAH] and is now found in the region along $\omega = +60°$. This is a graphic example that the absolute magnitude of the global potential energy of the minimum is not necessarily an indication of conformational restriction. Rather, it is the distribution of potential energy among the ensemble microstates that specifies to what extent molecules are localized in conformational space.

Figure 2 displays the volume of conformational space within which 95% of the population of molecules can be found for Ω[HSEA]. Again, essentially identical surfaces are observed for the other Ω's. These volumes are substantially larger than those specifying the 50% probability level (Figure 1) and are approximated by the available, sterically allowed, subset of Ω and hence differ little between alternate potential energy functions.

A more detailed representation of the population distribution amongst conformational microstates is shown in Figure 3 where semilogarithmic plots of F, the minimum fraction of Ω necessary to obtain the specified probability, are shown. These distribution curves fit

$$P = P_{max}/[1 + (a/F^b)]$$

Since P and F are normalized, the parameters a and b are sufficient to describe the curves. The parameter a corresponds to the value of F^b at the 50% probability level while b is indicative of the "steepness" of the distribution about a. Table I lists the fitted values of a and b for the various algorithms used. Inspection of Figure 3 and Table I shows two points worth noting. First, for all four potential energy algorithms tested, the number of microstates defining the subset of Ω within which there is a 95% probability of finding a given molecule is roughly 10% of the total whereas the 50% probability level accounts for about 1% of all conformational microstates. The number of sterically accessible microstates

Table II: Summary of Calculated ⟨NOE⟩'s and ⟨T_1⟩'s for the Man(α1,6) Linkage in Man(α1,6)Man(β)OMe[a]

		⟨NOE⟩'s					
				⟨NOE⟩ from algorithm			
irradiated hydrogen	detected hydrogen	observed NOE (%)	range ($\pm 2\sigma$)	HSEA	HEAH	HSEL	HSEH
Man6-H1	Man6-H2	13.0	12.0–14.0	15.9	15.9	14.0	14.2
	βMan-H6	4.0	3.4–4.6	4.2	3.9	4.6	3.8
	βMan-H6′	1.3	0.5–2.1	1.3	1.7	2.2	3.3
	βMan-H5	1.0	0.0–2.5	0.6	0.6	0.8	1.1
βMan-H5	βMan-H1	12.1	10.7–13.5	12.5	12.5	12.5	12.5
	Man6-H1	1.8	1.2–2.4	1.5	1.5	2.1	2.1

		⟨T_1⟩'s				
			⟨T_1⟩ from algorithm			
detected hydrogen	observed T_1 (s)	range (±20%)	HSEA	HEAH	HSEL	HSEH
Man6-H1	1.02	0.82–1.22	0.97	0.96	0.86	0.86
βMan-H1	0.62	0.50–0.74	0.72	0.72	0.72	0.72
βMan-H5	0.70	0.56–0.84	0.62	0.62	0.60	0.60
βMan-H6′	0.40	0.32–0.48	0.33	0.33	0.33	0.33

[a] Observed NOE and T_1 values were obtained on a 20 mM solution of the disaccharide in D_2O. τ_c for this sample was estimated to be 1.0×10^{-10} s. Observed NOE's are expressed as a percent of the saturated signal and are the average of four experiments. The specified range for NOE values is calculated as the average value ± two standard deviations.

is typically on the order of 10–20% of the total. Thus, the distribution is dominated by a large number of (relatively) high-energy microstates. For example, the distribution generated after utilization of the HSEA potential yields a 50% probability level by considering any microstate with an energy less than −0.7 kcal/mol (1.5 kcal/mol above the global minimum). The second point revealed by Figure 3 and Table I is that the relative depth of the global minima associated with the four potentials (−2 to −6 kcal/mol) apparently has little effect on the resulting population distribution among conformational microstates. Therefore, the different algorithms are, in a sense, self-correcting. Inclusion of a hydrogen-bonding term (in algorithms HEAH and HSEH) results in a reduction in the parameter b, that is, a slight sharpening of the distribution.

By utilizing the method outlined under Experimental Procedures, ⟨NOE⟩'s and ⟨T_1⟩'s were calculated for comparison with experimentally determined values. Calculated ⟨NOE⟩'s and ⟨T_1⟩'s are listed in Table II. The validity of the method is demonstrated by comparison of conformationally *in*sensitive ⟨NOE⟩'s and ⟨T_1⟩'s with experimentally derived values (e.g., ⟨βMan-H1{βMan-H5}⟩ and ⟨Man6-H2{Man6-H1}⟩ NOE's). With all four potential energy algorithms employed, excellent agreement is observed. This is to be expected since these values were used to estimate τ_c. Somewhat greater variation in the results is observed for calculated values of conformationally dependent interresidue enhancements (e.g., ⟨Man6-H1-{βMan-H5}⟩ and ⟨βMan-H6′{Man6-H1}⟩) among the various potentials used. In general, ensembles generated with algorithms including the exo-anomeric effect yield better agreement with experimental observations than those which include only van der Waals and electrostatic interactions. The close agreement between the ⟨NOE⟩'s calculated from Ω-[HSEA] and Ω[HEAH] is somewhat surprising since inclusion of hydrogen-bonding terms yields distinct alterations of local minima in potential energy surfaces, thus affecting the position in conformational space of the most significantly populated microstates. This again indicates that it is the population distribution in Ω and the nature of the variation in r^{-6} that are the dominant factors in determining ⟨NOE⟩ and ⟨T_1⟩ values, not necessarily the depth of the local (or global) potential energy minima.

One interaction not explicitly accounted for in these potential energy algorithms is the "Hassel–Ottar effect" (Hassel & Ottar, 1947). This effect is a syn-1,3 axial interaction which, in 6-O-substituted gluco-type hexopyranosides, occurs between O4 and O6 when $\omega = +60°$ (Marchessault & Perez, 1979). The magnitude of this interaction has been estimated to be on the order of +3 kcal/mol, a value that will dramatically reduce the fraction of the molecular population in the $\omega = +60°$ region [see Cumming and Carver (1987)]. In order to mimic this effect, ⟨NOE⟩'s and ⟨T_1⟩'s for each ensemble were recalculated with the region from $\omega = 0°$ to $+120°$ ignored ("truncated" data set) and Ω renormalized. ⟨NOE⟩'s and ⟨T_1⟩'s thus calculated were almost identical with those listed in Table II. This was expected since (1) the relatively high-energy microstates in the $\omega = +60°$ region should give only minor contributions to ensemble averaged observables and (2) in this particular linkage calculated NOE and T_1 values in this region are not highly sensitive to variations in ω.

The results presented in Table II are in agreement with those previously published for an analogous disaccharide, Man-(α1,6)Man(α)OMe (Brisson & Carver, 1983a). In that study, the only major interresidue enhancement observed was Man(αOMe)-H6{Man(α1,6)-H1}. This enhancement, in combination with bulk longitudinal relaxation times, allowed specification of the α1,6 torsional angles to the following values: $\phi = -50 \pm 20°$, $\psi = 90$–$200°$, and $\omega = -60°$ or $+180°$ (in roughly equal proportions). Because of the particular spectral characteristics of the βM residue of the disaccharide used in this study, an additional interresidue NOE and T_1 are available for definition of the glycosidic torsion angles of the α1,6 linkage, the Man6-H1{βMan-H5} enhancement and the βMan-H5 T_1. An "intersection surface" experimentally defining the solution conformation of the α1,6 linkage can be sought [see Cumming et al. (1987) for examples of this methodology] from the set of conformationally sensitive NMR relaxation data: the Man6-H1, βMan-H5, and βMan-H1 T_1's plus the βMan-H5{Man6-H1}, βMan-H6{Man6-H1}, βMan-H6′{Man6-H1}, and Man6-H1{βMan-H5} enhancements. However, intersection surfaces centered at $\phi, \psi = -65°, 175°$, with ω = either $-60°$ or $180°$, are observed only if selected data (e.g., Man6-H1{βMan-H5}) are ignored (data not shown); i.e., *no intersection surface is obtained if all the data are considered.* Therefore, no single conformer is consistent with all the data. On the other hand, averaging over all of Ω can yield ⟨NOE⟩'s and ⟨T_1⟩'s consistent with all observed data and thus confirms quantitatively the previous qualitative suggestion of conformational averaging over ψ and ω (Brisson & Carver, 1983a). From a comparison of the observed and calculated NOE's and T_1's (Table II), we conclude that the population distribution of α1,6 linkage conformers in solution

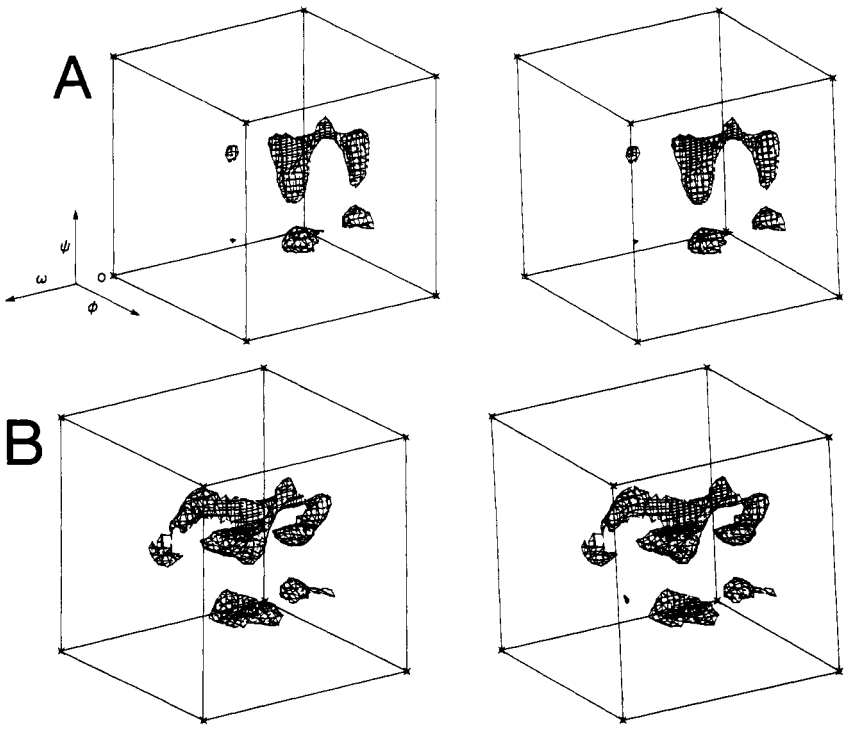

FIGURE 4: Three-dimensional contour surfaces representing the 50% population level in calculated ensembles for GlcNAc(β1,6)Man(α)OMe. Details for the presentation of these contour plots are given in the legend to Figure 1. Threshold energy levels were calculated to be inclusive of 50% of the disaccharide population. (A) HSEA: global minimum, −3.2 kcal/mol; MPL, 0.097%; threshold energy level, −1.8 kcal/mol. (B) HSEL: global minimum, −6.6 kcal/mol; MPL, 0.0581%; threshold energy level, −5.0 kcal/mol. For the other two ensembles calculated but not shown, the following data were obtained: (Ω[HEAH]) global minimum, −4.8 kcal/mol; MPL, 0.973%; threshold energy level, −2.2 kcal/mol; (Ω[HSEH]) global minimum, −8.1 kcal/mol; MPL, 0.409%; threshold energy level, −4.0 kcal/mol.

is best represented for this molecule by Ω[HSEA] or Ω-[HEAH] (the hydrogen-bond interaction term being of little influence) as shown in Figures 1 and 2.

The GlcNAc(β1,6) Linkage. In the first paper in this series (Cumming et al., 1987), experimentally determined values for the glycosidic torsion angles of this linkage were derived for the disaccharide GlcNAc(β1,6)Man(α)OMe. The angles ϕ and ψ were described by a range of values centered about 0° and 190° while two distinct rotameric subpopulations about the Manα C5–C6 bond, yielding values for ω of −60° and 180°, were found to be present. The value of ϕ is particularly unusual since β-linked hexopyranoses generally exhibit ϕ values near +50°.

These results again suggested averaging over a number of conformational states specified by multiple minima on a potential energy surface. Figure 4 illustrates two of the three-dimensional contour surface of Ω's calculated with the four algorithms described under Experimental Procedures. The contour level displayed corresponds to the threshold potential energy necessary to define 50% of the molecular population. The following points are worth noting upon inspection of Figure 4. (1) The 50% surfaces observed for Ω[HSEA] (Figure 4A) and Ω[HEAH] for this compound are qualitatively similar to those generated for compound I. These similar characteristics include the lack of appreciable population in ω = +60° region and the appearance of segmented population domains about two minima oriented along the ψ axis. (2) In contrast to compound I, considerable differences are evident in Ω[HSEL] and Ω[HSEH] relative to Ω[HSEA] and Ω-[HEAH]. The Ω[HSEL] (Figure 4B) displays considerable volume oriented along the ϕ axis in regions of conformational space, in this case including negative ϕ values, not observed for Ω[HSEA] and Ω[HEAH]. Moreover, differential effects are evident in the ω = +60° region, where in Figure 4B considerably more volume is evident in this region for Ω-[HSEL] than for Ω[HSEA]. (3) Again in contrast to compound I, inclusion of hydrogen-bonding terms in the potential energy algorithms yield more discernible effects. The 50% contour surfaces for Ω[HEAH] and Ω[HSEH] occupy a smaller volume of Ω than those without such a term (Figure 4). Again, a more detailed analysis of the population distribution confirms this observation (Table I and Figure 3B). Occupation of a small fraction of Ω is quantified in Table I by a reduction in the fitted parameters a and b, although the general distribution profiles for all four calculated Ω's are grossly similar to those calculated for compound I. (4) Unlike compound I, the global minimum for all ensembles, except Ω[HSEA], is located in the ω = +60° region. Inclusion of a positive potential energy term to account for unfavorable syn-axial (Hassel–Ottar) interactions would be insufficient to eliminate negative potential energy values from this region for these Ω's, although a greatly reduced fraction of the population would remain. Therefore, greater differences would be anticipated between ⟨NOE⟩'s and $\langle T_1 \rangle$'s calculated for the complete and the "truncated" ensembles.

⟨NOE⟩'s and $\langle T_1 \rangle$'s were again calculated for each ensemble; Table III lists the pertinent results. The conclusions drawn from calculations for the mannobioside discussed above do not apply here. While intraresidue enhancements (e.g., ⟨GlcNAc-H3{GlcNAc-H1}⟩, ⟨GlcNAc-H4,5{GlcNAc-H1}⟩) calculated for all four ensembles are in excellent agreement with observed values, calculated interresidue enhancements are in poor agreement except for Ω[HSEA], which yields a ⟨Man-H6{GlcNAc-H1}⟩ marginally lower than the experimental range allows. To ascertain whether the greater population in the ω = +60° region is sufficient to distort calculated ⟨NOE⟩'s and $\langle T_1 \rangle$'s, ensemble averaged observables were recalculated with the truncated data set. The calculated results (Table III) yield better agreement for Ω[HSEA] and Ω-[HEAH], but not for Ω[HSEL] and Ω[HSEH]. Therefore,

Table III: Summary of Calculated ⟨NOE⟩'s and ⟨T_1⟩'s for the GlcNAc(β1,6) Linkage in GlcNAc(β1,6)Man(α)OMe[a]

Complete Ensemble ⟨NOE⟩'s

irradiated hydrogen	detected hydrogen	observed NOE (%)	range (±2σ)	⟨NOE⟩ from algorithm HSEA	HEAH	HSEL	HSEH
GlcNAc-H1	Man-H6	1.6	1.2–2.1	0.9	0.9	1.7	2.4
	Man-H5,6′ + GlcNAc-H2	7.4	5.8–9.0	8.0	7.0	9.2	8.4
	GlcNAc-H3	5.7	4.5–6.9	6.5	6.5	6.5	6.5
	GlcNAc-H4,5	10.3	9.8–11.0	9.9	9.9	9.9	9.9
Man-H6	Man-H5,6′	30.3	28.8–31.9	29.2	28.3	28.1	26.6
	GlcNAc-H1	1.8	1.2–2.4	1.8	3.7	3.2	4.6

Complete Ensemble ⟨T_1⟩'s

detected hydrogen	observed T_1 (s)	range (±2σ)	⟨T_1⟩ from algorithm HSEA	HEAH	HSEL	HSEH
GlcNAc-H1	0.43	0.34–0.52	0.51	0.53	0.46	0.46
Man-H1	1.01	0.81–1.21	0.99	1.00	0.99	0.99
Man-H2	0.72	0.58–0.86	0.99	0.98	0.98	0.98
Man-H6	0.24	0.19–0.29	0.24	0.23	0.23	0.22

Truncated Ensemble ⟨NOE⟩'s

irradiated hydrogen	detected hydrogen	observed NOE (%)	range (±2σ)	⟨NOE⟩ from algorithm HSEA	HEAH	HSEL	HSEH
GlcNAc-H1	Man-H6	1.6	1.2–2.1	1.4	1.0	2.0	2.6
	Man-H5,6′ + GlcNAc-H2	7.4	5.8–9.0	6.9	7.5	8.2	7.3
	GlcNAc-3	5.7	4.5–6.9	6.5	6.5	6.5	6.5
	GlcNAc-H4,5	10.3	9.8–11.0	10.0	10.0	10.1	10.0
Man-H6	Man-H5,6′	30.3	28.8–31.9	30.3	29.9	29.8	29.1
	GlcNAc-H1	1.8	1.2–2.4	2.0	3.0	3.9	5.1

Truncated Ensemble ⟨T_1⟩'s

detected hydrogen	observed T_1 (s)	range (±2σ)	⟨T_1⟩ from algorithm HSEA	HEAH	HSEL	HSEH
GlcNAc-H1	0.43	0.34–0.52	0.52	0.53	0.47	0.48
Man-H1	1.01	0.81–1.21	0.99	0.99	0.98	0.98
Man-H2	0.72	0.58–0.86	0.98	0.98	0.98	0.98
Man-H6	0.24	0.19–0.29	0.23	0.23	0.23	0.22

[a] Observed NOE and T_1 values are taken from Table II in the preceding paper. Observed NOE's are the average of five or six experiments. The specified range for NOE values is calculated as the average value ± two standard deviations. The truncated ensemble is derived by omitting all microstates with ω values between 0° and 120°.

the poor agreement observed with Ω[HSEL] and Ω[HSEH], principally manifested in ⟨GlcNAc-H1{Man-H6}⟩, is not the result of omission of Hassel–Ottar effects but rather is due to the regions of conformational space sampled by these ensembles. As demonstrated in the first paper in this series (Cumming et al., 1987), an NOE or T_1 surface can be calculated as a function of the glycosidic torsion angles. Indirectly, the topological features of these surfaces are a reflection in conformational space of the intrinsic molecular geometry and can hence be useful in rationalizing the effect of averaging over r^{-6}. As can be readily appreciated by inspection of any of the calculated surfaces, different enhancements can possess distinct ϕ–ψ–ω surfaces and will thus yield ⟨NOE⟩ values that are differentially sensitive to the Boltzmann weighting of the population distribution. It is also worthy of note that, in both cases, Ω's calculated with algorithms incorporating hydrogen-bonding interactions are in poorer agreement than for Ω's omitting this interaction. The significance of this observation will be discussed further below.

On the basis of these results and those presented in the preceding paper, it is therefore possible to classify the NMR-defined solution conformation for this 1,6 linkage, determined in the first paper in this series, as virtual: it is an artifactual conformation derived by averaging over multiple conformational states and which, in itself, describes only an insignificant fraction of the population of disaccharide molecules. By analogy with Man(α1,6)Man(β)OMe, averaging in ψ results in an apparent value of 190°, which, in the simplest case (i.e., the population distribution in Ω[HSEA]), is due to two minima (conformers) at ψ = 95° and 256°. Invoking the simplest case is supported by the observation that ⟨NOE⟩ and ⟨T_1⟩ values calculated from population distributions derived from the HSEA potential yield the best overall agreement with experimental results, although the presence of a higher number of averaging conformers cannot be eliminated.

Extension to Other Types of Glycosidic Linkages. Since the solution conformation of 1,6 linkages, such as those in the disaccharides described above, can only be adequately defined by the population distribution in an appropriate Ω, the question arises whether identical conclusions can be made for other glycosidic linkages (e.g., 1,2, 1,3, or 1,4). Or, as was previously done (Brisson & Carver, 1983; Carver et al., 1987), can the solution conformation defined by the intersection surface of conformationally sensitive NOE's and T_1's adequately describe the dominant conformations?

The 1,2 linkage in the disaccharide GlcNAc(β1,2)Man(α)OMe will be used as an example. HSEA potential energy calculations yield a single, well-defined minimum at ϕ, ψ = 48°, 19°, whereas inclusion of a hydrogen-bonding term results in the appearance of an additional quasi-equivalent minimum centered at ϕ, ψ = 54°, −3° (Figure 5). However, unlike the trisaccharide GlcNAc(β1,2)[GlcNAc(β1,6)]Man(α)OMe [see Cumming et al. (1987) and Cumming and Carver (1987)], the NMR-defined conformation for the GlcNAc(β1,2) linkage in this disaccharide exclusively overlaps neither of these minima; the intersection surface appears as a thin strip falling between the two minima with a range of ϕ, ψ values centered at 50°, 10° (Cumming and Carver, unpublished observations). This implies averaging in ψ between the two minima for this disaccharide. Two NOE experiments yield the necessary conformationally dependent enhancements to evaluate the solution conformation of this linkage: GlcNAc-H1{Man-H2}

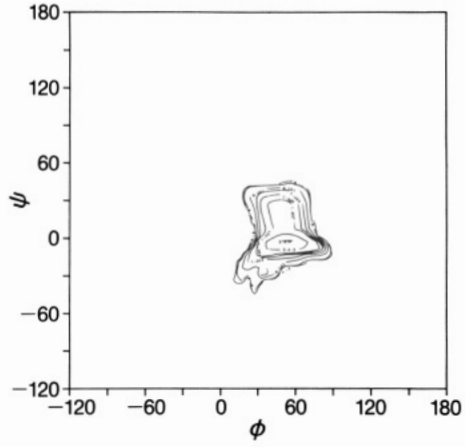

FIGURE 5: Isoenergy contour surfaces for the β1,2 linkage in GlcNAc(β1,2)Man(α)OMe. Negative potential energy surface maps, as a function of ϕ and ψ for rotation about the GlcNAc(β1,2) linkage, were calculated as described under Experimental Procedures. In this figure, the 12 contour levels are defined as the following percentages of the minimum (most negative) value in the array: 99.0, 95.0, 85.0, 75.0, 65.0, 55.0, 45.0, 35.0, 25.0, 15.0, 5.0, and 3.0. Potential energies were calculated with the HEAH algorithm. Two minima are observed. A local minimum at $\phi, \psi = 48°, 19°$ of −2.1 kcal/mol is observed that corresponds to the HSEA-calculated global minimum. However, for this ensemble, a global minimum (−4.0 kcal/mol) at $\phi, \psi = 54°, -3°$ is evident. The surface calculated with the HSEL algorithm (not shown) yields two minima, one at $\phi, \psi = 19°, 36°$ (−5.6 kcal/mol) and another at $\phi, \psi = -14°, -26°$ (−4.2 kcal/mol), while the surface calculated with the HSEH algorithm shows a new global minimum of −6.1 kcal/mol located at $\phi, \psi = 54°, -2°$ (although the two HSEL minima are still present). The additional energy increments calculated with the HSEH and HEAH algorithms arise solely from the formation of a hydrogen bond between the ring oxygen of the Gn residue and the C3 OH of the Man residue.

and Man-H2{GlcNAc-H1}. In addition, the T_1 values of the GlcNAc-H1, Man-H2, and Man-H1 are also conformationally dependent. ⟨NOE⟩ and ⟨T_1⟩ values were calculated from the corresponding set of two-dimensional ensembles generated with the four potential energy functions, described under Experimental Procedures, and compared with experimental results.

Table IV shows the results of these calculations. Again, for all four ensembles, intraresidue ⟨NOE⟩'s (e.g., ⟨GlcNAc-H3{GlcNAc-H1}⟩, ⟨GlcNAc-H4,5{GlcNAc-H1}⟩, and ⟨Man-H1{Man-H2}⟩) are all in good agreement with observed values. Considerable variation is observed in the magnitude of conformationally sensitive, interresidue ⟨NOE⟩'s (e.g., ⟨Man-H2{GlcNAc-H1}⟩ and ⟨GlcNAc-H1{Man-H2}⟩). This variation is a reflection of the different population distributions for each Ω. Moreover, only Ω[HSEA] yields calculated results that are in complete agreement with observed values for interresidue enhancements. In addition, both ensembles generated with potential energy algorithms that include contributions from hydrogen-bond interactions are in poorer agreement than their counterparts, which omit this interaction. The basis of these observations is clearly understood by inspection of the calculated potential energy surfaces for each ensemble. The HSEA and HEAH algorithms mimic the exo-anomeric effect by modulating the potential energy as a function of ϕ. This is accomplished by adding positive energy increments at ϕ values displaced from +50° (for β-linked hexapyranoses) or −50° (for α-linked hexopyranoses). The isoenergy contour surfaces generated by the HEAH algorithm is shown in Figure 5. For both the HSEA and HEAH algorithms, inclusion of the exo-anomeric effect results in localization of negative potential energies to regions centered about $\phi = 50°$. The effect of including a hydrogen-bonding term (Figure 5) is to alter the ψ value for the minimum as well

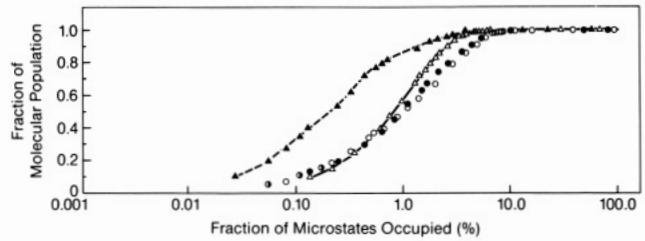

FIGURE 6: Calculated population distribution among conformational microstates in GlcNAc(β1,2)Man(α)OMe. Semilogarithmic plot shows the minimum fraction of the total number of ensemble lattice points (3600) necessary to account for the specified fraction of the population of disaccharide molecules. (△) HSEA potential energy algorithm; (○) HSEL potential energy algorithm; (●) HSEH potential energy algorithm; (▲) HEAH potential energy algorithm. Note the evident left shift of the HEAH curve. Further characteristics of these curves are presented in Table I.

as its depth. On the other hand, the HSEL algorithm generates an isoenergy contour map exhibiting two minima, one of which occurs at a negative ϕ value, and exhibiting regions of negative potential energy over a much larger segment of the ϕ–ψ surface (data not shown). Further addition of a hydrogen-bonding term (HSEH algorithm) creates a new global minimum at $\phi, \psi = 52°, -2°$. For each of these ensembles, the corresponding isoprobability contour surfaces can be calculated as described under Experimental Procedures. Three points deserve comment. First, Ω[HSEL] and Ω-[HSEH] possess population distributions distinct from Ω-[HSEA] and Ω[HEAH] where, in the former ensembles, a considerable fraction of the molecular population is found in regions of the ϕ–ψ surface with ϕ values less than 30°. Second, the major effect of including a hydrogen-bonding term is to shift the ϕ–ψ position for the majority of the population of molecules. This shift results in the differences observed in ⟨NOE⟩'s calculated from Ω's generated with and without hydrogen-bonding terms. Third, the population distribution in this linkage is not markedly different than that encountered for 1,6 linkages (Figure 6). The majority of the population of molecules is associated with regions of the ϕ–ψ surface that possess negative potential energy. Except for Ω[HEAH], 50% of the molecular population occupy about 1% of available microstates while 95% of the population occupy 10%, approaching the limit of sterically accessible microstates. That the Ω[HEAH] population distribution does not represent a meaningful model for the solution conformation of this linkage is of considerable interest since it implies that, like the previous two examples, hydrogen-bond formation does not play an appreciable role in determining the conformations of this linkage. As is evident in Figure 6, the population distribution for this ensemble occupies a much smaller fraction of the ensemble microstates than the others; a significant "left shift" is evident for this ensemble. This suggests that formation of this hydrogen bond may not be energetically favorable due to a substantial entropic penalty, manifested in this case by a reduction in occupied microstates at the 50% level. This interpretation is discussed below.

Application of Ensemble Averaging to the β1,2 Linkage in GlcNAc(β1,2)[GlcNAc(β1,6)]Man(α)OMe. In the preceding paper (Cumming et al., 1987), we concluded that the solution conformation of the GlcNAc(β1,2) linkage in the trisaccharide GlcNAc(β1,2)[GlcNAc(β1,6)]Man(α)OMe was stabilized by the presence of an interresidue hydrogen bond between the Man C3 hydroxyl and the GlcNAc(β1,2) ring oxygen. Figure 7 illustrates the relationship of the NMR-derived solution conformation for the β1,2 linkage to the results of potential energy calculations. Figure 7A shows the isoenergy surface

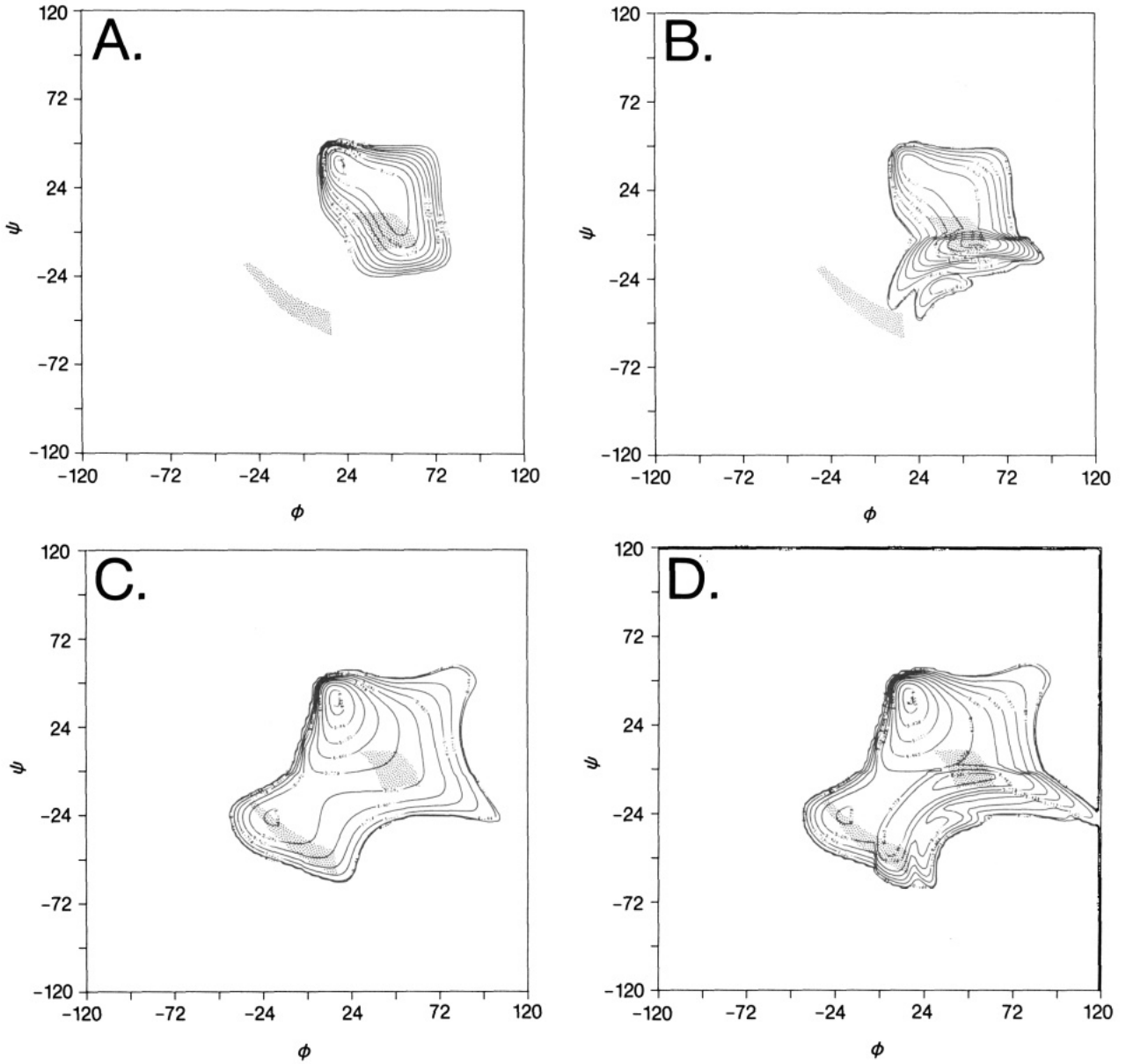

FIGURE 7: Negative potential energy contour maps for the GlcNAc(β1,2) linkage in the trisaccharide GlcNAc(β1,2)[GlcNAc(β1,6)]Man(α)OMe. The potential energy surface was calculated with values for the GlcNAc(β1,6) linkage torsion angles fixed at ϕ, ψ, ω = 55°, 190°, −60°. The shaded area on each surface shows the two NMR-derived solution conformations for this linkage. (A) Potential energy surface calculated utilizing a HSEA potential. A global minimum of −2.7 kcal/mol is observed at ϕ, ψ = 22°, 38° with a second, quasi-equivalent minimum near ϕ, ψ = 45°, 28°. (B) Potential energy surface calculated with the HEAH potential. A new global minimum of −4.3 kcal/mol is observed at ϕ, ψ = 56°, −4°, although the depth and position of the previously described minima are unchanged. (C) Surface calculated using a HSEL potential. Two minima of −6.9 kcal/mol (ϕ, ψ = 16°, 40°) and −3.8 kcal/mol (ϕ, ψ = −20°, −24°) are observed. (D) Negative energy surface calculated with a HSEH potential. Three minima are now evident. Two (including the global minimum) remain at the previously described ϕ, ψ values, with identical depths, but an additional minimum (−5.2 kcal/mol) is now present at ϕ, ψ = 42°, −6°. The additional negative energy increments observed in panels B and D are due to hydrogen-bond formation between the GlcNAc(β1,2) ring oxygen and the Man C3 hydroxyl. This minimum overlaps the intersection surface experimentally determined (in the first paper in this series, Figure 5) as the solution conformation for this linkage.

obtained with the HSEA potential. Two quasi-equivalent minima (−2.7 kcal/mol) occur at ϕ, ψ = 45°, 28° and 22°, 38°. The former minimum corresponds to the anticipated local minimum predicted from the exo-anomeric effect (ϕ values near +50° for a β-linked hexopyranose). The latter minimum results from favorable van der Waals interactions between acetamido methyl groups in the two GlcNAc(β) residues. The NMR-determined solution conformations overlap neither of these minima. Figure 7B shows the contour surface obtained with the HEAH potential. While the previous two local minima are still present, a new global minima (−4.3 kcal/mol) is observed at ϕ, ψ = 56°, −4°. The additional energy increments seen in Figure 7B are solely due to one hydrogen-bond interaction between the GlcNAc(β1,2) ring oxygen and the Man C3 hydroxyl (O...O distance = 2.78 Å at the new global minimum). This new minimum overlaps one of the NMR-determined intersection surfaces. The isoenergy contour surfaces calculated with the HSEL and the HSEH potentials are shown in panels C and D of Figure 7, respectively. In Figure 7C, a global minimum of −6.9 kcal/mol is observed at ϕ, ψ = 16°, 40°, again due to favorable van der Waals and electrostatic interactions between the acetamido moieties of the two GlcNAc(β) residues. Inclusion of a hydrogen-bonding interaction term (Figure 7D) yields the same incremental energy levels observed in Figure 7B but in this case does not result in formation of a new global minimum. However, one of the NMR-derived intersection surfaces is again observed to overlap this new minimum. Given the nature of these

Table IV: Summary of Calculated ⟨NOE⟩'s and ⟨T_1⟩'s for the GlcNAc(β1,2) Linkage in GlcNAc(β1,2)Man(α)OMe and GlcNAc(β1,2)[GlcNAc(β1,6)]Man(α)OMe[a]

GlcNAc(β1,2)Man(α)OMe ⟨NOE⟩'s

				⟨NOE⟩ from algorithm			
irradiated hydrogen	detected hydrogen	observed NOE (%)	range (±2σ)	HSEA	HEAH	HSEL	HSEH
GlcNAc-H1	GlcNAc-H2	3.4	2.2–4.6	4.8	4.3	4.1	4.2
	GlcNAc-H3	8.1	6.5–9.7	8.0	8.0	7.9	7.9
	GlcNAc-H4,5	12.8	11.2–14.4	12.5	12.5	12.7	12.7
	Man-H1	7.5	6.0–9.0	8.7	3.4	9.7	5.1
	Man-H2	10.0	8.4–11.6	10.6	12.5	14.1	15.1
Man-H2	Man-H1	7.8	6.2–9.4	8.1	10.0	6.8	8.7
	Man-H3	14.2	13.2–15.2	16.5	16.4	16.4	16.3
	GlcNAc-H1	9.2	7.2–11.2	7.8	10.5	10.3	12.4

GlcNAc(β1,2)Man(α)OMe ⟨T_1⟩'s

			⟨T_1⟩ from algorithm			
detected hydrogen	observed T_1 (s)	range (±20%)	HSEA	HEAH	HSEL	HSEH
GlcNAc-H1	0.46	0.36–0.56	0.54	0.59	0.47	0.52
Man-H1	0.82	0.66–0.98	0.84	1.03	0.74	0.92
Man-H2	0.69	0.55–0.83	0.75	0.72	0.68	0.66

GlcNAc(β1,2)[GlcNAc(β1,6)]Man(α)OMe ⟨NOE⟩'s

				⟨NOE⟩ from algorithm			
irradiated hydrogen	detected hydrogen	observed NOE (%)	range (±2σ)	HSEA	HEAH	HSEL	HSEH
GlcNAc-H1	GlcNAc-H2	2.8	1.8–3.8	2.8	2.8	2.7	2.7
	GlcNAc-H3	4.0	2.0–6.0	3.8	3.8	3.8	3.8
	GlcNAc-H4,5	5.6	3.6–7.6	5.7	5.7	5.7	5.7
	Man-H1	nd[b]		4.8	2.4	5.7	5.1
	Man-H2	7.6	4.8–10.4	4.8	5.3	5.8	6.0
Man-H2	Man-H1	4.2	2.2–6.2	3.2	4.0	2.6	2.9
	Man-H3	5.3	2.9–7.7	6.9	6.9	6.9	6.9
	GlcNAc-H1	5.0	3.8–6.2	3.3	4.3	3.8	4.1

GlcNAc(β1,2)[GlcNAc(β1,6)]Man(α)OMe ⟨T_1⟩'s

			⟨T_1⟩ from algorithm			
detected hydrogen	observed T_1 (s)	range (±20%)	HSEA	HEAH	HSEL	HSEH
GlcNAc2-H1	0.47	0.29–0.65	0.45	0.51	0.39	0.40
Man-H1	0.87	0.70–1.04	0.64	0.78	0.55	0.59
Man-H2	0.80	0.64–0.96	0.66	0.64	0.61	0.60

[a] Observed NOE and T_1 values were taken either from Table II in the preceding paper (for the trisaccharide) or from our own unpublished results (for the disaccharide). Column labels have the same meaning described for the previous two tables. [b] nd, NOE not detected due to proximity of signal to residual HDO.

potential energy surfaces and the results presented above (especially those concerned with hydrogen bonding), we applied the ensemble averaging protocol to evaluate the validity of our conclusions about the solution conformations of this linkage drawn in the preceding paper.

Again, population contour surfaces were calculated for each Ω shown in Figure 7. The results of these calculations can be summarized as follows. The population distribution for Ω[HSEA] is such that, to characterize the linkage conformation for 96% of the population, a considerable range of ϕ (6°–75°) and ψ (−24°–50°) must be considered. The range of ϕ–ψ values required to specify 50% of the population is somewhat smaller (ϕ = 12°–55°; ψ = 2°–45°) but still much larger than that specified by the "intersection" surface defined for this linkage in the preceding paper. For Ω[HEAH], possible values of ϕ (30°–68°) and ψ (−6° to 0°) are much more restricted for 50% of the population but are again very large for the remaining fraction. For both Ω[HSEL] and Ω[HSEH], large ranges of possible ϕ–ψ values are observed. The additional hydrogen-bonding interaction used to calculate Ω[HSEH] does not result in a significant restriction of possible torsion angle values, in contrast to Ω[HEAH].

⟨NOE⟩'s and ⟨T_1⟩'s were calculated for the four generated ensembles. The results are listed in Table IV. In contrast to the disaccharides, complete agreement with observed relaxation data was obtained only with Ω[HEAH] (i.e., when hydrogen-bonding interactions are explicitly calculated). For Ω[HSEA], the ⟨Man-H1 T_1⟩ (0.64 s) and ⟨GlcNAc2-H1{Man-H2}⟩ (3.3%) were found to lie outside the experimentally determined limits (the ⟨NOE⟩ value is 3σ from the mean) while for Ω[HSEL] and Ω[HSEH] two of the conformationally sensitive ⟨T_1⟩ values (for Man-H1 and Man-H2) lie outside the experimental limits. Therefore, in this case the population distribution of Ω[HEAH] is the best representation of the solution conformation of the GlcNAc(β1,2) linkage in this trisaccharide. Even so, in this distribution only 68% of the population of conformers form an intramolecular hydrogen bond. It is worth noting that although this example represents the narrowest, experimentally verified population distribution we have observed to date, the experimentally determined intersection surface (see previous paper) overlaps only a portion of the ensemble, corresponding to 44% of the molecular population. Hence, the majority of molecules in solution possess torsion angles outside the limits of the experimentally determined intersection surface in all examples considered.

Population Distribution for the GlcNAc(β1,2) Linkage in GlcNAc(β1,6)[GlcNAc(β1,2)]Man(α)OMe Is Dependent upon Other Glycosidic Torsion Angles. The results presented above are not definitive since the potential energy surfaces shown in Figure 7 are affected by additional degrees of freedom, namely, the GlcNAc(β1,6) torsion angles. Neglect of this influence could have important consequences upon the population distribution and hence the calculated values of ⟨NOE⟩'s and ⟨T_1⟩'s. For example, for Ω[HSEA] only a single parameter, the ⟨GlcNAc2-H1{Man-H2}⟩ NOE, is in substantial disagreement with experimental observations. Therefore, any

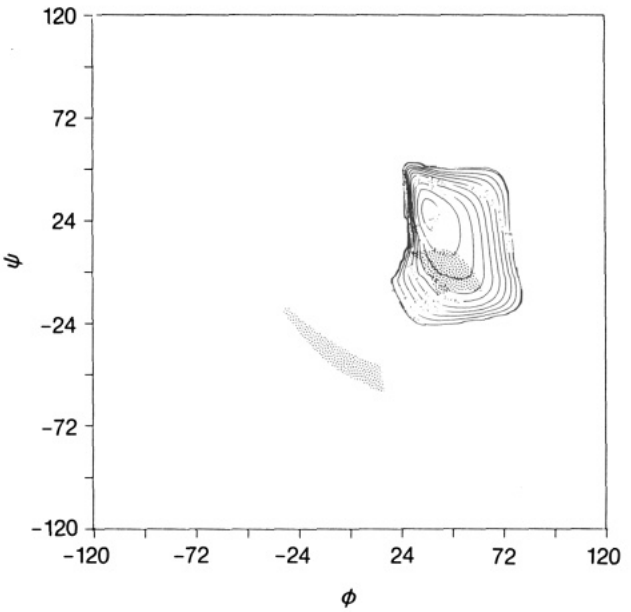

FIGURE 8: Negative potential energy contour map for the GlcNAc(β1,2) linkage in the trisaccharide GlcNAc(β1,2)-[GlcNAc(β1,6)]Man(α)OMe. Details for the calculation of this map are the same as described in the legend to Figure 5. The potential energy surface was calculated with values for the GlcNAc(β1,6) linkage torsion angles fixed at ϕ, ψ, ω = 40°, 190°, −60°. The shaded area on the surface shows the two NMR-derived solution conformations for this linkage. A HSEA potential was used to calculate this energy surface. The well reaches a minimum of −3.4 kcal/mol at ϕ, ψ = 38°, 28°.

redistribution of the conformer population could raise the magnitude of this parameter and alter conclusions about the utility of hydrogen-bonding interactions.

To illustrate the sensitivity of the potential energy surfaces of the GlcNAc(β1,2) linkage to alterations in the GlcNAc-(β1,6) torsion angle ϕ, the surface shown in Figure 7A has been recalculated (Figure 8) by holding the GlcNAc(β1,6) ϕ at 40° instead of its minimum energy value of 55°. This simple change in ϕ (ΔE = +0.3 kcal/mol) results in the elimination of the local or global minimum at ϕ, ψ = 16°, 40°, as a result of unfavorable steric interactions between the two GlcNAc(β) acetamido groups. Inspection of isoprobability contour plots calculated from surfaces such as that in Figure 8 shows a marked redistribution for all ensembles, except Ω[HEAH], compared to the isoprobability surfaces calculated from the data in Figure 7 (data not shown).

However, ⟨NOE⟩'s and ⟨T_1⟩'s calculated from the ensembles where the GlcNAc(β1,6) ϕ = 40° (e.g., Figure 8) yield no significant alterations when compared to values calculated where the GlcNAc(β1,6) ϕ = 55°. For Ω[HSEA], the calculated value (3.2%) of ⟨GlcNAc2-H1{Man-H2}⟩ is identical with that obtained when the GlcNAc(β1,6) ϕ = 55° and thus still differs considerably from that observed experimentally (5.0%). That identical calculated values for this ⟨NOE⟩ were obtained from both Ω[HSEA]'s is more clearly understood by comparison of Figure 5 of the preceding paper (the NOE contour surface shown in that figure is in fact that calculated for the Man-H2{GlcNAc2-H1} NOE; however, the topological features of the GlcNAc2-H1{Man-H2} NOE surface are similar to that in Figure 5) with Figures 7A and 8 in this paper. A line connecting the two minima at ϕ, ψ = 16°, 40° and 45°, 28° runs nearly parallel to the contour lines shown for this NOE (Figure 5, preceding paper). Therefore, any redistribution of the population upon changes in the GlcNAc(β1,6) ϕ value will not result in any major alteration of calculated ⟨NOE⟩'s. While this is a fortunate coincidence in this case, it underlines the importance of identifying all degrees of freedom that affect the population distribution in an ensemble. For this trisaccharide, rigorous determination of ensemble-averaged observables requires, at a minimum, calculation of a seven-dimensional lattice, each dimension corresponding to a glycosidic torsion angle. We are currently seeking methods to assess a higher dimension conformational space in a computationally tractable manner. While conclusions drawn from static subsets of conformational space are thus tentative, we believe our results valid in this case since all sources of significant perturbation of potential energy have been identified and evaluated.

Discussion

The major conclusion of this paper is that the utility of NMR in determining the solution conformation of glycans is to test population distributions predicted by empirical potential energy functions. Solution conformation studies yield, at best, a self-consistent representation whose veracity is demonstrable only by *quantitative* analysis of ensemble averaged observables. Alternative population distributions in conformational space are equally acceptable as long as they meet this sole experimental criterion; it is not possible to systematically preclude the existence of other population distributions. Therefore, all previous quantitative conformational analyses of glycans, including those from this laboratory, are erroneous to the extent that the majority of the molecular population possesses linkage conformations not defined by the NMR-derived solution conformation.

Previous approaches to the quantitative determination of the solution conformation, from NMR-derived data alone, have focused on determining the range of conformations, *any one of which* could account for the observed data (Brisson & Carver, 1983a–c). Thus, although molecular flexibility was implicitly assumed, it was not accounted for in calculating NOE's and T_1's. The intention of this study was to assess whether the neglect of internal motions implicit in our previous method of treating relaxation data was justifiable. The current treatment shows that such an approach is not valid and that explicit potential energy functions must be used to evaluate ensemble averaged relaxation data. As a result, NMR data can still be used to evaluate potential energy functions, but ensemble average NOE's and T_1's must be compared to the observed data.

The goal of this paper was to *quantitatively* assess the effects of internal motions on the determination of the solution conformation of glycans. In all four examples considered herein, averaging the calculated relaxation data over the ensemble of conformational microstates, according to a normalized probability determined for each microstate by a Boltzmann distribution, yields averaged values in agreement with experimental data if an appropriate potential energy algorithm is used. In all of these examples, the values of experimentally observed relaxation data can be seen to be derived from a nontrivial relationship in conformational space between the population distribution, a function of the distribution of potential energy among ensemble microstates, and the NOE or T_1 surface, itself a complex function of the intrinsic molecular geometry. A similar approach has been utilized by Perez and co-workers (Perez et al., 1985) to evaluate transglycosidic $^3J_{H-C}$ coupling constants of maltose in various solvents. Good agreement was found between experimentally observed coupling constants and those calculated from a Boltzmann probability distribution of conformers.

Several additional points are worthy of note. First, the wide range of ϕ–ψ–ω values available in a given linkage confor-

mation is largely a reflection of the shallow rotational potential energy surfaces for these glycosidic linkages. For small oligosaccharides (three or less monosaccharide residues), these surfaces are typically only 2–4 kcal/mol deep. Since the majority of the molecular population (80–98%) is usually found within 2 kcal/mol of the global minimum, all of the necessary microstates are energetically accessible just from random thermal motion (assuming 0.6 kcal/mol per degree of freedom). Nevertheless, it should be further noted that the absolute magnitude of a global minimum does not necessarily dictate a more confined population distribution. In the case of Man(α1,6)Man(β)OMe, certain potential energy algorithms yielded a global minimum approaching −7.0 kcal/mol yet generated population distributions nearly identical with other algorithms yielding minima on the order of −2.5 to −3.0 kcal/mol. It is the distribution of potential energy among ensemble microstates that dictates the population distribution in conformational space.

Second, in light of these results, our understanding of what is meant by a solution conformation should be redefined. Clearly our previous quantitative approach is inadequate. Such terms as "preferred orientation" and "linkage conformation" are also inappropriate since the fraction of the molecular population specified by a given set of torsion angles, even at the potential energy minimum, is exceedingly small (<1%; see the maximum probability found for any ensemble microstate, MPL, listed in the legend to Figures 1 and 4). All of these approaches are grounded in the notion that a single (or relatively few) defined conformation(s) exist(s) in solution. As demonstrated here, solution conformations can only be described in terms of population distributions in conformational space.

Third, it is observed that, for the disaccharides studied in this paper, ensemble averaged observables calculated from algorithms that include hydrogen-bonding terms are in substantially poorer agreement with experimental results than those produced without hydrogen-bonding terms. Two possibilities could account for this observation. First, the maximum energetic magnitude (−2 kcal/mol) for this interaction may be overestimated in these compounds. Reducing the maximum magnitude of this interaction would have the effect of reducing the distortions in ⟨NOE⟩'s and ⟨T_1⟩'s observed. However, arbitrarily reducing the magnitude of this interaction must be viewed at this point with some suspicion. Second, these potential energy algorithms ignore solvent effects, especially competition for hydrogen-bond formation with water. In addition, thermodynamic contributions, such as those arising from conformational entropy, are also not considered. However, since excellent agreement in all of these cases can be obtained with Ω[HSEA], the fact remains that there is no experimental justification for invoking hydrogen-bond interactions for these compounds.

Fourth, for the GlcNAc(β1,2) linkage in the trisaccharide GlcNAc(β1,2)[GlcNAc(β1,6)]Man(α)OMe, the distribution of potential energy among ensemble microstates (and hence the population distribution for this ensemble) is dependent upon additional degrees of freedom, notably that of the ϕ torsion angle in the GlcNAc(β1,6) linkage. When this ϕ possesses values near 40°, a marked reduction in the number of sterically accessible microstates for the GlcNAc(β1,2) linkage occurs. In principle, this could result in a proportionally higher weighting of ϕ–ψ values with larger GlcNAc2-H1{Man-H2} values. However, in this case it was demonstrated that contributions from the fraction of the molecular population with GlcNAc(β1,6) ϕ values near 40° did not raise the magnitude of ⟨GlcNAc2-H1{Man-H2}⟩ (and ⟨Man-H1 T_1⟩) to within experimentally acceptable limits. Nonetheless, this example clearly indicates the necessity of evaluating the effect of all degrees of freedom upon the rotational potential energy for a given linkage.

Finally, two observations suggest that the range of torsion angle values in larger N-linked glycans will be more restricted. The first observation is that, at the 98% population level, the number of significantly occupied ensemble microstates is dictated by steric limitations. Since glycans are branched structures, it would be anticipated the number of sterically allowed microstates would decrease as the number of branches and constituent monosaccharide residues increases. Our preliminary calculations on high-mannose and complex-type tri-, tetra-, and pentaantennary glycans indicate that this is indeed the case (Cumming and Carver, unpublished observations). Furthermore, in contrast to the disaccharide examples, Ω[HEAH] for the GlcNAc(β1,2)[GlcNAc(β1,6)]Man(α)OMe trisaccharide gave the best agreement between experimental and calculated ⟨NOE⟩'s and ⟨T_1⟩'s. The formation of a hydrogen bond significantly restricts the number of populated microstates in this trisaccharide. An example of this restriction is most easily seen in Figure 6, where the Ω[HEAH] curve for the disaccharide GlcNAc(β1,2)Man(α)OMe is shifted to the left by an order of magnitude. The quantitative consequence of the analogous shift in the GlcNAc(β1,2)[GlcNAc(β1,6)]Man(α)OMe trisaccharide can be seen if one considers the minimum area of conformational space inclusive of 50% of the molecules. Without a hydrogen bond, this would correspond to an area within a radius of approximately 30° of the global minimum; with a hydrogen bond this area is confined to a radius of 6°. In larger branched sugars, where the possibility often exists for several hydrogen bonds to form, one might expect that the distribution of the majority of conformations about some linkages may be restricted to a few degrees. Under the latter circumstances, one would be justified in refering to these as single stable conformers. However, it should be noted that one cannot deduce the presence of such highly restricted states, a priori, from NMR data. Instead, it is necessary to calculate ensemble averaged observables for comparison to experimental data.

ACKNOWLEDGMENTS

We thank Dr. Art Grey, Dr. Brad Bendiak, Dr. Jim Rini, and Steven Michnick for stimulating discussions and advice. We are grateful to Dr. Serge Perez for making his hydrogen-bonding algorithm available to us prior to its publication.

Registry No. Man(α1,6)Man(β)OMe, 100896-85-3; GlcNAc-(β1,6)Man(α)OMe, 80264-88-6; GlcNAc(β1,2)Man(α)OMe, 55797-38-1; GlcNAc(β1,2)[GlcNAc(β1,6)]Man(α)OMe, 109976-96-7.

REFERENCES

Bloembergen, N. (1971) *Nuclear Magnetic Relaxation*, Benjamin, New York.

Brisson, J. R., & Carver, J. P. (1983a) *Biochemistry 22*, 1362–1368.

Brisson, J. R., & Carver, J. P. (1983b) *Biochemistry 22*, 3671–3679.

Brisson, J. R., & Carver, J. P. (1983c) *Biochemistry 22*, 3680–3686.

Carver, J. P., Cumming, D. A., & Grey, A. A. (1987) in *Glycoprotein Structure and Conformation* (Ivatt, R. J., Ed.) Plenum, New York (in press).

Cumming, D. A., & Carver, J. P. (1987) *Biochemistry* (third paper of three in this issue).

Cumming, D. A., Shah, R. N., Krepinsky, J. J., Grey, A. A., & Carver, J. P. (1987) *Biochemistry* (first paper of three in this issue).
Dais, P., Shing, T. K. M., & Perlin, A. S. (1984) *J. Am. Chem. Soc. 106*, 3082-3089.
Gueron, M., Chachaty, C., & Son, T.-D. (1973) *Ann. N.Y. Acad. Sci. 222*, 307-323.
Jardetzky, O. (1980) *Biochim. Biophys. Acta 621*, 227-232.
Jardetzky, O., & Roberts, G. C. K. (1981) *NMR in Molecular Biology*, Academic, New York.
Keepers, J. W., & James, T. L. (1982) *J. Am. Chem. Soc. 104*, 929-939.
Kitaigorodsky, A. I. (1961) *Tetrahedron 14*, 230-236.
Kitaigorodsky, A. I. (1978) *Chem. Soc. Rev. 7*, 133-163.
Lemieux, R. U., Bock, K., Delbaere, L. T. J., Koto, S., & Rao, V. S. (1980) *Can. J. Chem. 58*, 631-653.
Mackie, W., Sheldrick, B., Akrigg, D., & Perez, S. (1986) *Int. J. Biol. Macromol. 8*, 43-51.
Marchessault, R. H., & Perez, S. (1979) *Biopolymers 18*, 500-521.
Noggle, J. H., & Schirmer, R. E. (1971) *The Nuclear Overhauser Effect*, Academic, New York.
Perez, S., Taravel, F., & Vergelati, C. (1985) *Nouv. J. Chim. 9*, 561-564.
Potenzone, R., & Hopfinger, A. J. (1975) *Carbohydr. Res. 40*, 322-336.
Ramachandran, G. N., & Sasisekharen, V. (1968) *Adv. Protein Chem. 23*, 283-437.
Rees, D. A., & Scott, W. E. (1971) *J. Chem. Soc. B*, 469-479.
Shah, R. N., Cumming, D. A., Grey, A. A., Carver, J. P., & Krepinsky, J. J. (1986) *Carbohydr. Res. 153*, 155-161.
Thorgersen, H., Lemieux, R. U., Bock, K., & Meyer, B. (1982) *Can. J. Chem. 60*, 44-57.
Tvaroska, I., Perez, S., & Marchessault, R. H. (1978) *Carbohydr. Res. 61*, 97-106.
Venkatachalam, C. M., & Ramachandran, G. N. (1967) in *Conformation of Biopolymers* (Ramachandran, G. N., Ed.) Vol. I, p 83, Academic, New York.
Woessner, D. E., Snowden, B. S., & Meyer, G. H. (1969) *J. Chem. Phys. 59*, 719-721.

Reevaluation of Rotamer Populations for 1,6 Linkages: Reconciliation with Potential Energy Calculations†

Dale A. Cumming and Jeremy P. Carver*
Departments of Medical Genetics and Medical Biophysics, University of Toronto, Toronto, Ontario, Canada M5S 1A8
Received May 28, 1986; Revised Manuscript Received April 3, 1987

ABSTRACT: Applications of ensemble averaging to the solution conformation of model compounds for N-linked glycans are further investigated. Specifically, the interpretation usually applied to observed values of $J_{5,6'}$, a parameter reflecting the rotameric distribution about C5-C6 bonds (torsion angle ω in 1,6 glycosidic linkages) in 6-O-substituted hexopyranosides, was found to be inconsistent with populations derived from potential energy calculations. However, agreement between observed and calculated, ensemble-averaged values of $J_{5,6'}$ was obtained and the distribution of ω rotamers reinterpreted. Values of $J_{5,6'}$ that were previously interpreted as indicative of equipartition between two rotamers in fact reflect a marked preference for one of them. Additional potential energy terms, previously absent from energy calculations, are introduced and shown to be without effect on interpretations of ω rotamer distributions. From comparisons with both NMR relaxation and scalar coupling constant data, it is concluded that a simple empirical algorithm, HSEA, calculating van der Waals, exo-anomeric, and (as appropriate) hydrogen-bonding terms, is best suited for describing the population distributions in solution for oligosaccharides and N-linked glycans.

In the previous paper (Cumming & Carver, 1987), we demonstrated that analysis of the solution conformation of glycans is predicated, first and foremost, upon potential energy calculations, which allow determination of the distribution of conformers about a given linkage in solution. Because they are averages, constraints upon internuclear distances determined by NMR[1] may not realistically reflect those present in solution. Thus, the utility of NMR in such investigations is to confirm calculated population distributions. In this paper, we extend our ensemble calculations to another NMR parameter of principle import to glycan conformational analysis, investigate the effects upon population distributions in conformational space of other interaction terms frequently absent from potential energy algorithms, and illustrate a situation where even ensemble averaging fails to account for the experimentally observed population of conformers in solution.

Experimental Procedures

Computational Procedures. Methods for the calculation of steric interactions and rotational potential energies were presented in the preceding (Cumming & Carver, 1987). Contributions to the potential energy due to the "Hassel-Ottar" (HO) effect (Hassel & Ottar, 1947; Marchessault & Perez, 1979) were also calculated in conjunction with the four potential energy algorithms. The HO contribution, as a

† This research supported by Grants MT-3732 and MA-6499 from the Medical Research Council of Canada.
* Address correspondence to this author.

[1] Abbreviations: HO, Hassel-Ottar effect; Man, D-mannopyranose; GlcNAc, 2-acetamido-2-deoxy-D-glucopyranose; NMR, nuclear magnetic resonance spectroscopy; SDDS, spin-decoupling difference spectroscopy; COSY, homonuclear shift correlated spectroscopy; HSEA, van der Waals + exo-anomeric effect; HSEL, van der Waals + electrostatic; HEAH, van der Waals + exo-anomeric effect + hydrogen bonding; HSEH, van der Waals + electrostatic + hydrogen bonding; PFM, potential function methods; MPL, maximum (normalized) probability of any microstate in an ensemble.

0006-2960/87/0426-6676$01.50/0